Tellus

The influence of large-scale atmospheric circulation on the variability of salinity at Helgoland Roads station

The influence of large-scale atmospheric circulation on the variability of salinity at Helgoland Roads station

Monica IONITA[1*], Gerrit LOHMANN[1], Norel RIMBU[1], Karen WILTSHIRE[2]

[1] Alfred Wegener Institute for Polar and Marine Research, Bremerhaven, Germany

[2] Alfred Wegener Institute for Polar and Marine Research, Helgoland, Germany

Address:

Alfred Wegener Institute

Bussestrasse 24

D-27570 Bremerhaven

Germany

Telephone: +49(471)4831-1845

[1]

[1] *Corresponding author:
e-mail: Monica.Ionita@awi.de

AB STRACT

The variability of April salinity at Helgoland Roads station (54.12°N, 7.9ºE, Germany) is analyzed in relationship with Elbe river discharge and the observed variability in large-scale atmospheric circulation for the period 1962-2000. It is shown that the main driver of salinity anomalies is the river discharge anomalies from the previous month. These discharge anomalies are strongly related with precipitation anomalies from the Elbe catchment area. Changes in the salinity, discharge and precipitation anomalies are accompanied by a wave-train atmospheric circulation pattern that connects the tropical Atlantic Ocean and northern part of Europe, as well as with changes in large-scale water vapour transport over the whole German Bight. Positive sea surface temperature anomalies centred in the Caribbean region and the North Sea are associated with positive salinity anomalies and negative anomalies of discharge and precipitation.

1. Introduction

The eastern German Bight is a zone of intensive mixing of two water bodies, the North Sea water and the coastal water which is of lower salinity and density. In addition, the water of the river Elbe leads to a strong inhomogeneity in this area which can be seen in the distribution of salinity and nutrients Goedecke (1968). During the last decade interest in the variability of hydrological (i.e. river run-off) and ecological parameters (salinity, nutrients) in connection with large-scale atmospheric circulation has markedly increased (Aebischer et al., 1990, Dippner, 1997a, b; Becker and Pauly, 1996). The interannual variability in observed ecological time series is sometimes suspected to be driven by interannual variability in climatic parameters (Fromentin and Planque, 1996).

Cushing and Dickson (1976) speculated that atmospheric circulation is responsible for a series of events that were observed in the North Sea in the last few decades. He showed that the beginning and end of an anomalously strong and long-lasting high pressure system over Greenland correspond with the so-called "Russell cycle" (Russell et al., 1971; Russell, 1973). According to his hypothesis the breakdown of this high pressure system at the end of 1960s led to changes in the wind stress and induced the Great Salinity Anomaly (GSA) (Dickson et al, 1988). The cool, low-stratified water columns of the GSA delayed the primary production (phytoplankton) and thus led to changes in the food web.

Other studies focused on the whole German Bight identified that on annual timescales, 90% of the observed salinity variability is in phase and correlated with a lag of several months to large-scale air pressure (Heyen and Dippner, 1998). Schott (1966) and Dickson (1971) revealed a connection between salinity variations in the North Sea and the atmospheric circulation, though both authors disagreed on the mechanism. While Schott (1966) found evidence that the surface salinities in the entire North Sea are dominated by large-scale

atmospheric advection via precipitation, Dickson (1971) suggested that advection of haline Atlantic waters is the main cause.

The goal of this study is to investigate the possible relationships between the large-scale atmospheric circulation and salinity, at Helgoland Roads station (54.12ºN, 7.9ºE, Germany) for the period 1962-2000. Understanding the causes of salinity variability: (i) will help to reconstruct historical salinities in connection with the atmosphere-ocean dynamics and (ii) will allow the study of the variability of other ecological time series (i.e. nutrients) in connection with the large-scale circulation, due to the fact that salinity anomalies are supposed to coincide with observed changes in the ecosystem (Nehring, 1994; Lindeboom et al., 1995).

The paper is organized as follows. The data sets used in this study are described in section 2. The results are presented in section 3. A summary and the main conclusions follow in section 4.

2. Data

In 1962 a long-term pelagic monitoring program observing nutrients, salinity and plankton species composition at Helgoland was initiated by the Biologische Anstalt Helgoland (Hickel et. al, 1993; Hickel, 1998). The measurements were made on a daily basis, except weekends. Helgoland Roads station (Figure 1) is situated approximately 60 km of the mouth of Elbe River, which is the most important source of fresh water input. In this study we used the daily salinity data from which we computed the monthly means for the period 1962-2000.

Elbe River discharge data (German Hydrological Institute, BfG, Kobelnz) measured at Neu-Darchau (53º23'N, 10º87'E) was also used for this study. From the daily data sets we

compute the monthly means for discharge. The average March discharge of Elbe river, for the

period analyzed in this study, is 1024 m^3/s.

In the analysis we used the following large-scale variables:

a) Monthly Sea Level Pressure (SLP) on a 5º×5º grid from the reanalysis data of the

National Centre for Atmospheric Research (NCAR) (Trenberth and Paolino, 1980), updated

version.

b) Monthly Sea Surface Temperature (SST) on a 5º×5º grid (Kaplan et. al, 1998), for

the 170ºW to 170ºE and 40ºS to 90ºN area. The data set have been update to year 2000.

c) The vertically integrated water vapour transport (WVT) (eq. 1) (Peixoto and Oort,

1992) for the period 1962–2000, calculated using zonal wind (u), meridional wind (v) and

specific humidity (q):

$$\vec{Q}(\lambda,\phi,t) = Q_\lambda \vec{i} + Q_\phi \vec{j} \qquad \text{eq. (1)}$$

Where zonal (Q_λ) and meridional (Q_Φ) components of Q are given by:

$$
\begin{aligned}
Q_\lambda &= \int_0^{p_0} qu \frac{dp}{g} \\
Q_\phi &= \int_0^{p_0} qv \frac{dp}{g}
\end{aligned}
\qquad \text{eq. (2)}
$$

For each vertical layer and each grid-point of NCEP/NCAR model we calculate the

product between the daily values of horizontal wind and specific humidity (q) corresponding

to lower and upper pressure level (p), respectively. The result is multiplied with the pressure

difference corresponding to lower and upper layer and divided by gravity. The WVT is

obtained by summation of water transport for all layers located between the earth's surface

and 300 hPa level. Above 300 hPa the specific humidity in the NCEP/NCAR model is zero

(Kalnay et al., 1996).

We also used the divergence of water vapour Q, which is in balance with the surface

fresh water flux E-P (Starr and Peixoto, 1958; Peixoto and Ort, 1992):

$$\nabla \bullet \vec{Q} = E - P \, ,$$

where ∇ denotes the two dimensional divergence operator, E evaporation and P precipitation. Regions of mean positive divergence (E-P>0) constitute source regions of water vapour, meanwhile the regions of convergence (E-P<0) are sink regions for water vapour.

d) Gridded precipitation data from the Climatic Research Unit (CRU) with 0.5ºx0.5º horizontal resolution (Mitchell et al., 2003). This data set (CRU TS 2.1) is based on precipitation observations at meteorological stations corrected for inhomogeneities in the station records. From the CRU precipitation data we defined an *index for March precipitation* which covers the Elbe river catchments area (5ºE to 20ºE and 47ºN to 53ºN), as the averaged normalized precipitation over this region.

All the data sets used in this study are for the common period 1962-2000 and have been detrended and normalized, with respect to their standard deviation, prior to the analysis.

3. Results

3.1. EOF Analysis

In a first step, the correlation of Helgoland salinity and large-scale variables is calculated. Just April mean salinity was retained for this study, due to the fact that the highest correlation between salinity and large-scale circulation is found for this month (not shown) and the highest variability in the salinity time series was identified for April (Figure 2). Taking into account that the cross-correlation between the river discharge and salinity is highest when Elbe leads salinity with 14-24 days (Figure 3) we used for our study March river discharge.

The dominant pattern of variability in the salinity, Elbe discharge and precipitation time series is calculated through Empirical Orthogonal Function (EOF) analysis. EOF

technique (e.g.von Storch and Zwiers, 1999) aims at finding a new set of variables that capture most of the observed variance from the data through a linear combination of the original variables. The EOF method also served as a data-filtering procedure to smooth the noise in the data sets.

The EOFs are constructed using the normalized and detrended time series of April salinity, March Elbe discharge and the precipitation index for the period 1962-2000. The associated time series (PC1) was normalized by its standard deviation.

The first EOF (Figure 4a), which explains 71.23% of the total variance, captures an out-of phase relation between salinity and Elbe discharge and precipitation. This pattern implies that positive anomalies of salinity are associated with negative anomalies of Elbe discharge and precipitation and *vice versa*. The associated time coefficient (PC1) (Figure 4b) is highly correlated with Elbe discharge and salinity time series (Table 1).

3.2 Composite analysis

Given the significant relationship between the first principal component (PC1) and salinity, discharge and precipitation, we will show further just the composite maps between PC1 with SLP, SST and WVT fields.

To identify the physical mechanism responsible for the connection between PC1 and large-scale atmospheric circulation, we constructed the composite maps between PC1 and SLP for the years of high (> 0.75), respectively low (<-0.75) values of PC1. This threshold was chosen as a compromise between the strength of the climate anomalies associated to flow anomalies and the number of maps which satisfy this criteria. Further analysis has shown that the results are not sensitive to the exact threshold value used for our composite analysis.

For the years when PC1 < -0.75 (Figure 5a) we obtain a tripole-like pattern with positive centres over northern Europe and the Atlantic Ocean centred at 50ºW and negative anomalies centred over the Mid-Atlantic Ocean, centred at 18ºW. This tripole pattern in the SLP field resembles the jet guide identified by Hoskins and Ambrizzi (1993). According to them by putting a forcing in the vicinity of the North Atlantic jet stream maximum (40ºN, 75ºW), will produce a propagating wave train in the North Atlantic jet with a extension in the Arabian Gulf, as well as, a Eurasian extension. The anticyclone pattern over the northern part of Europe is consistent with low precipitation and high salinities. Anticyclonic activity over the German Bight blocks a large-scale advection of marine air to Europe and causes reduced precipitation (Heyen and Dipnner, 1998).

The tripole-like pattern in the SLP field is associated with a tripole-like pattern in the composite of PC1 with SST (Figure 5b). A similar SST pattern was identified by Deser and Blackmon (1993). Positive SST anomalies over the north tropical Atlantic are associated with negative SLP anomalies and anomalous lower cyclonic circulation over the subtropical latitudes. This can be attributed to the weakening of the Hadley circulation (suppressed ascending air over the equatorial region and descending air over the sub-tropics) (Handoh et al., 2006). The associated wind anomalies weaken the prevailing easterly winds, which in turn reduces surface evaporation, maintaining a positive SST anomaly (Sutton et al., 2000; Handoh et al., 2006). For the years when PC > 0.75 we obtain a pattern like the one in Figures 5a, b but with opposite signs (Figures 6a, b). The cyclonic pattern over the northern part of Europe induces high precipitation, high discharge and low salinity anomalies. This pattern is accompanied by westerly winds and the advection marine air, which causes intense precipitation in the western part of Europe.

To better assess the relationship between salinity variability in the Helgoland area and large-scale atmospheric circulation, we investigated the moisture transport in the North

Atlantic regions for the years with PC1 > 0.75 and PC1 < -0.75 standard deviation. Vector plots of the vertically integrated water vapour transport composites show that during years with PC1 < 0.75 (Figure 7a) a significant reduction of the water vapour transport downstream the whole German Bight and a shift of the axis of water vapour transport north-west of the North Sea is obvious. For the case when PC1 > 0.75 (Figure 7b) the axis of maximum moisture transport is directed from the Atlantic to the German Bight, which causes high precipitation anomalies and low salinity anomalies over this region. An intense convergent zone can be found over the western part of Europe, including Elbe's river catchment area, which causes intense precipitation and low salinity. This convergent zone associated with the low pressure pattern identified in the SLP field, suppresses evaporation and induces intense precipitation and low salinity.

4. Summary and conclusions

In this study we investigated the relation between large-scale atmospheric circulation and variability of salinity and Elbe river discharge. The main features of our study can be summarized as follows. High salinities levels (low discharge anomalies) are associated with a triple-like pattern in SLP and SST fields. The SLP pattern associated with positive salinity anomalies resemble the wave train identified by Hoskins and Ambrizzi (1993) in the North Atlantic jet stream. Positive anomalies of salinity (low discharge anomalies) are associated with an anticyclone pattern over Western Europe which causes reduced precipitation leading to higher salinity levels. Low salinity levels (high discharge anomalies) are associated with a cyclonic circulation over Western Europe which causes high precipitation. The SST pattern associated with high salinity anomalies (low discharge) has a triple-like structure. Positive SST anomalies over northern tropical Atlantic are associated with negative SLP anomalies

and anomalous lower cyclonic circulation over the subtropical latitudes that can be attributed to the weakening of the Hadley Cell circulation with suppressed ascending air over the equatorial region and descending air over the sub-tropics (Handoh et al., 2006).

The vertically integrated water vapour transport composites show that during years with high salinity anomalies (low discharge anomalies) there is a significant reduction of the moisture transport through the whole German Bight and a shift of the axis of moisture transport north-west of the North Sea and the European continent, which causes low precipitation over Western Europe. Low salinity anomalies are associated with an intense convergent zone over the western part of Europe, which induces high precipitation anomalies and suppresses evaporation.

Establishing a relationship between salinity variability, river discharge and large scale atmospheric circulation, might be a step forward in understanding the influence of climate on ecological parameters in the Helgoland area (i.e. nutrients), taking into account that most of these parameters are sensitive to changes in the salinity concentration and to the inputs from the Elbe river discharge (Nehring, 1994; Lindeboom et al., 1995; Fromentin and Planque, 1996).

A next step will be to study the variability of ecological time series at Helgoland Roads station in connection with atmospheric circulation and the variations in the salinity concentration.

References

Aebischer, N.J., Coulson, J.C. and Colebrook, J.M. 1990. Parallel long-term trends across four marine trophic levels and weather. *Nature* **347**,753–755.

Becker, G.A. and Pauly M. 1996. Sea surface temperature changes in the North Sea and their causes, *ICES J. Mar. Sci.* **53,** 887–898.

Cushing, D.H. and Dickson, R.R. 1976. The biological response in the sea to climate change. *Adv. Mar. Biol.* **14**, 1–122

Deser, C. and Blackmon, M.L. 1993. Surface Climate Variations over the North Atlantic Ocean during Winter: 1900-1989. *Journal of Climate* **6**, 1743-1753.

Dickson, R. R. 1971. A recurrent and persistent pressure-anomaly pattern as the principle cause of intermediatescale hydrographic variation in the European shelf-seas. *Dt. Hydrogr. Zt*. **24**, 97–119.

Dickson, R. R., Meincke, J., Malmberg, S.A. and Lee, A.J. 1988. The "Great salinity anomaly" in the Northern Atlantic 1968-1982, *Prog. Oceanog.* **20**, 103-151.

Dippner, J.W. 1997a. Recruitment success of different fish stocks in the North Sea in relation to climate variability. *Dtsch. Hydrogr. Zt.* **49**, 277–293.

Dippner, J.W., 1997b. A note on SST anomalies in the North Sea in relation to the North Atlantic Oscillation and the potential influence on the theoretical spawning time of fish. *Dt. Hydrogr. Zt.* **49**, 267–275.

Fromentin, J.M. and Planque, B. 1996. *Calanus* and environment in the eastern North Atlantic. II. Influence of the North Atlantic Oscillation on *C. finmarchicus* and *C. helgolandicus*. *Mar. Ecol. Prog. Ser.* **134**,111–118.

Goedecke, E. 1968: Über die hydrographische Struktur der Deutschen Bucht im Hinblick auf die Verschmutzung in der Konvergenzzone. Helgoländer wissenschaftliche Meeresuntersuchungen **17,** 108–125.

Handoh, I.C., Matthews, A.J., Bigg, G.R. and Stevens, D.P. 2006. Interannual variability of the tropical Atlantic independent of and associated with ENSO: Part I. The North Tropical Atlantic. *International Journal of Climatology* **26,** 1937-1956.

Heyen, H. and Dippner, J. W. 1998. Salinity in the southern German Bight estimated from large-scale climate data. *Tellus* **50A,** 545–556.

Hickel, W. 1998. Temporal variability of micro and nanoplankton in the German Bight in relation to hydrographic structure and nutrient changes. *ICES J. Mar. Sci.* **19**, 600-609.

Hickel, W., Mangelsdorf, P. and Berg, J. 1993. The human impact on the German Bight: Eutrophication during three decades (1962–1991). *Helgoländer Meeresunters* **47**, 243–263.

Hoskins, B. J. and Ambrizzi, T. 1993. Rossby wave propagation on a realistic longitudinally varying flow. *J. Atmos. Sci*. **54**, 1661–1671.

Kalnay, E., Kanamitsu, M., Kistler, R., Collins, W., Deaven, D., Gandin, L., Iredell, M., Saha, S., White, G., Woollen, J., Zhu, Y., Chelliah, M., Ebisuzaki, W., Higgins, W., Janowiak, J., Mo, K. C., Ropelewski, C., Wang, J., Leetmaa, A., Reynolds, R., Jenne, R. and Joseph, D.1996. The NMC/NCAR 40-Year Reanalysis Project. *Bull. Amer. Meteor. Soc.* **77**, 437-471.

Kaplan A, M.A. Cane, Y. Kushnir, A.C. Clement, M.B. Blumenthal, and B. Rajagopalan, 1998: Analyses of global sea surface temperature 1856–1991. *J. Geophys. Res.,* **9**, 18 567–18 589.

Lindeboom, H., van Raaphorst, W., Beukema, J., Cadebae, G. and Swennen, C. 1995. Sudden changes in the North Sea and Wadden Sea: Oceanic influences underestimated? *Dt. Hdrogr. Zt.* (**suppl. 2**), 87–100.

Mitchell, T.D., T.R. Carter, P.D. Jones, M. Hulme, and M. New 2003: A comprehensive set of high-resolution grids of monthly climate for Europe and the globe: The observed record (1901-2000) and 16 scenarios (2001-2100). *Tyndall Center Working Paper*, **55**, available online at http://www.tyndall.ac.uk/publications/working_papers/wp55.pdf

Nehring, S. 1994. Gymnodinium catenatum Graham (Dinophyceae) in Europe: A growing problem?. *J. Plankton Res.* **17**, 85–102.

Peixoto, J. P., and Oort, A. H. 1992. Physics of Climate, 520 pp., Springer, New York.

Russel, F.S. 1973. A summary of the observations on the occurrence of planktonic stages of fish off Plymouth 1924-1972. *Journal of the Marine Biological Association of the United Kingdom* **53**, 347-355.

Russel, F.S., Southward, A.J., Boalch, G.T. and Butler, E.I. 1971. Changes in biological conditions in the English Channel off Plymouth during the last half century. *Nature* **234**, 468-470.

Schott, F. 1966. Der Oberflächensalzgehalt in der Nordsee. *Dt. Hydrogr. Zt.* (**suppl. A9**),1–58.

Starr, V. and Peixoto, J. 1958. On the global water vapour and the hydrology o deserts. *Tellus* **10**, 189-194.

von Storch, H. and Zwiers, F. W. 1999. Statistical Analysis in Climate Research, 494 pp., *Cambridge Univ. Press*, New York.

Sutton, R.T., Jewson, S.P. and Rowell, D.P. 2000. The elements of climate variability in the tropical Atlantic region. *Journal of Climate* **13**, 3261-3284.

Trenberth, K. E. and Paolino, D. A. 1980. The Northern Hemisphere sea-level pressure data set: Trends, errors and discontinuities. *Mon. Wea. Rev.* **108**, 855-872.

Table 1. Correlation coefficients between PC1 and April salinity, March Elbe discharge and

March PP index

PC1	
Salinity	-0.78
Elbe Discharge	0.84
PP CRU	0.91

Figure captions

Figure 1. Location of Helgoland Roads station (black square) and the catchment area of Elbe river (Potsdam Institute for Climate Impact Research and River Basin Community Elbe)

Figure 2. Standard deviation of salinity at Helgoland Roads station for the period 1962-2000

**Figure 3.** Lag-correlation between daily Elbe river discharge and salinity (the 95% significance level is indicated with the dash-dotted line)

**Figure 4.** a) First EOF based on the normalized time series of April salinity, March Elbe river discharge and March PP Index and b) The corresponding coefficient time series (PC1) and salinity and discharge normalized time series

Figure 5. Composite map between PC1 (<-0.75) and (a) SLP, (b) SST. Units are hPa and K, respectively

Figure 6. Composite map between PC1 (>-0.75) and (a) SLP, (b) SST. Units are hPa and K, respectively

Figure 7. Composite maps of the vertically integrated water vapour transport for low (a) and high (b) values of PC1. Units are kg/(ms). The shaded areas indicate the distribution of the horizontal divergence of the total water vapour transport (units 10^{-6} kg/m^{2}s)

Figure 1. Location of Helgoland Roads station (black square) and the catchment area of Elbe river (Potsdam Institute for Climate Impact Research and River Basin Community Elbe)
207x232mm (96 x 96 DPI)
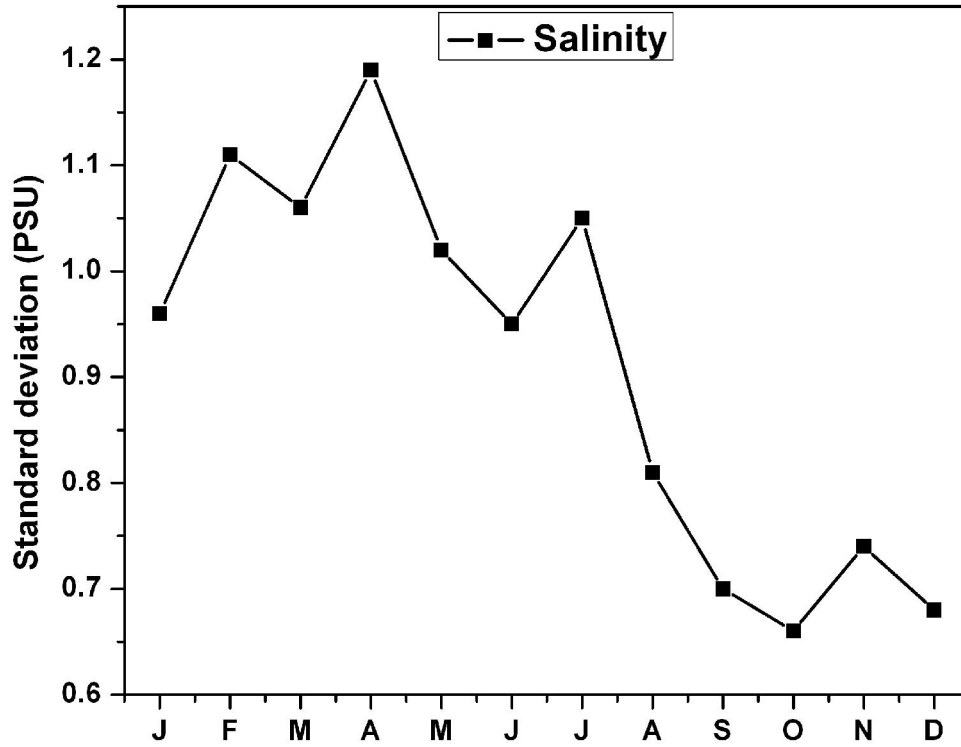
Figure 2. Standard deviation of salinity at Helgoland Roads station for the period 1962–2000
901x698mm (72 x 72 DPI)
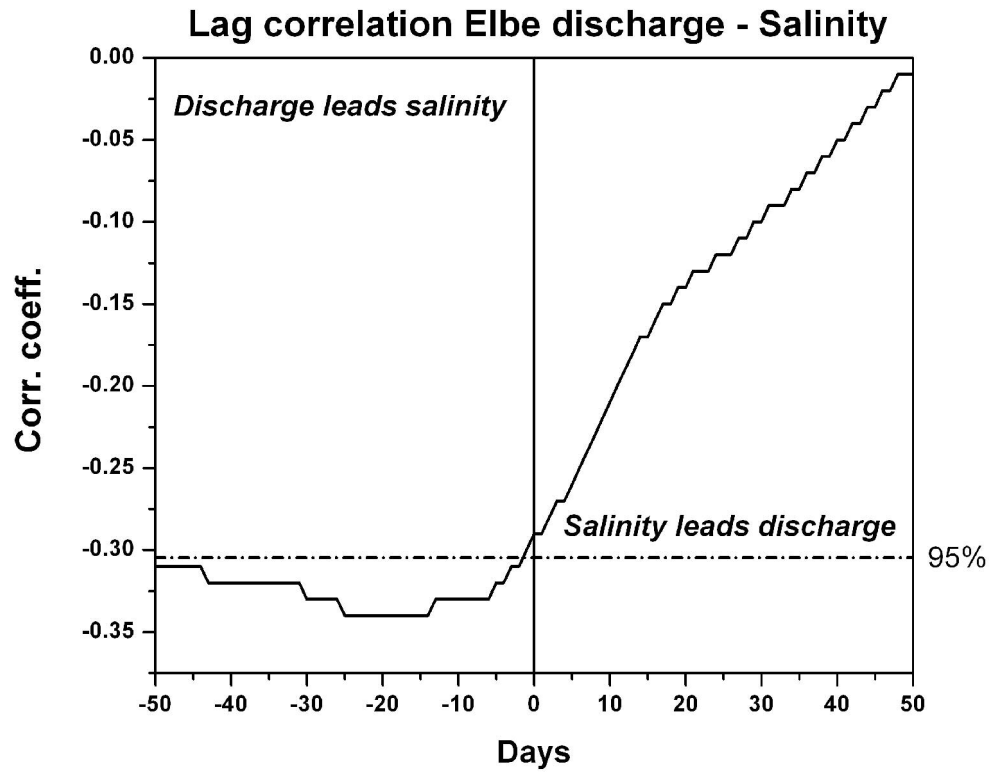
Figure 3. Lag-correlation between daily Elbe river discharge and salinity (the 95% significance level is indicated with the dash-dotted line)
241x192mm (300 x 300 DPI)
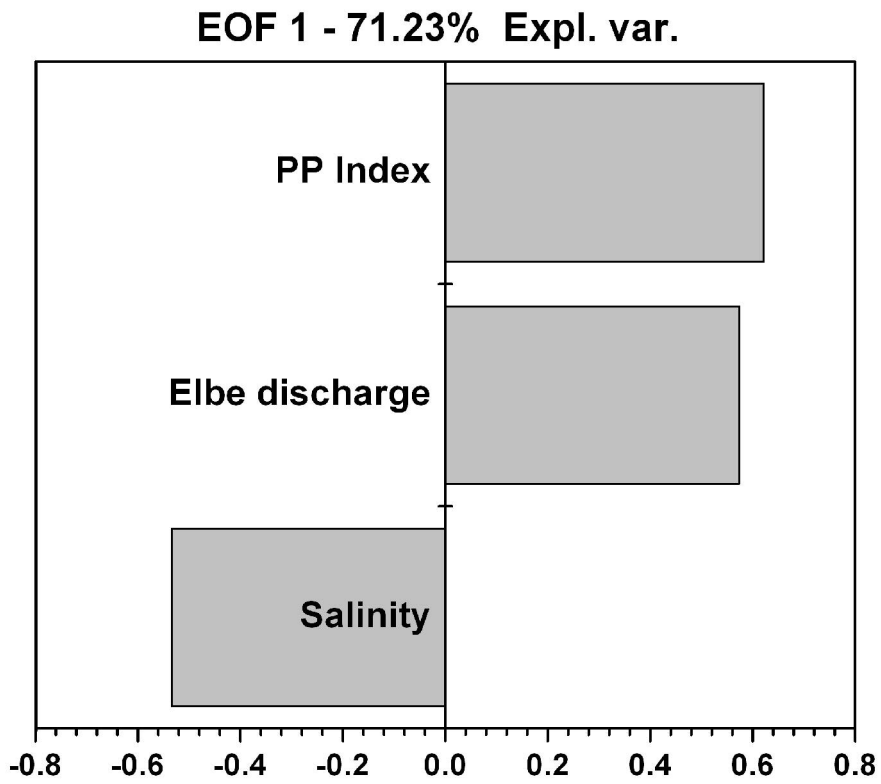
Figure 4. a) First EOF based on the normalized time series of April salinity, March Elbe river discharge and March PP Index
223x205mm (300 x 300 DPI)
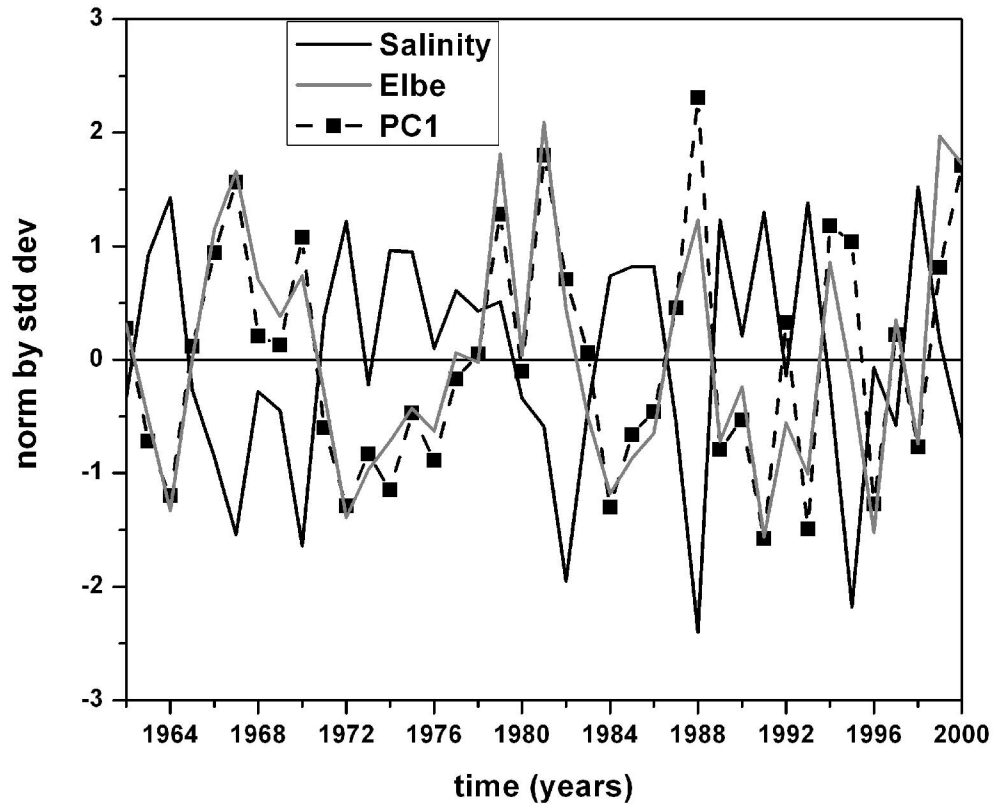
Figure 4. b) The corresponding coefficient time series (PC1) and salinity and discharge normalized time series
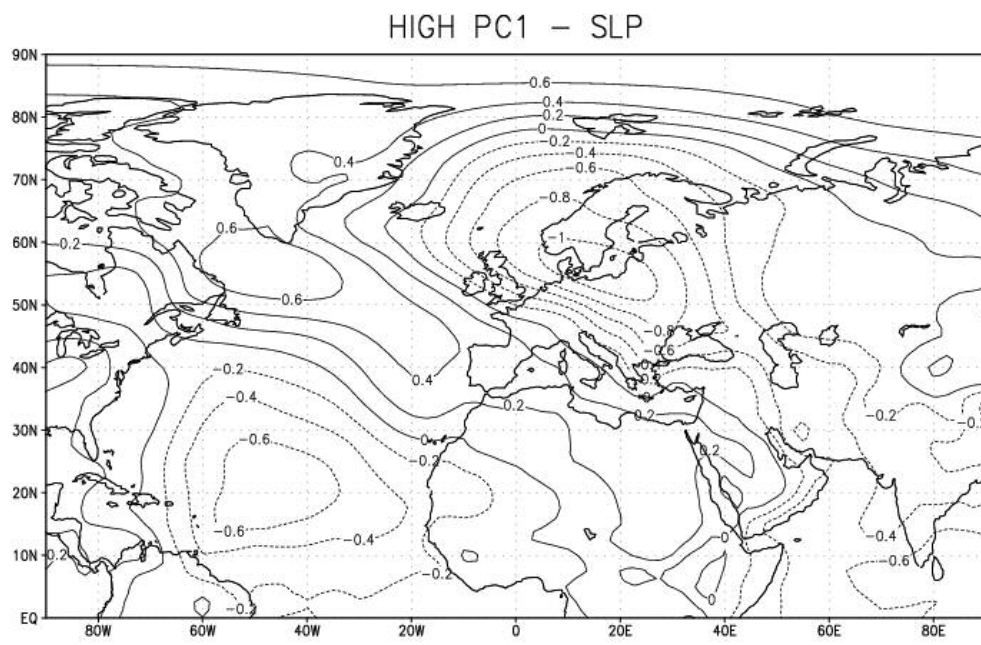911x739mm (72 x 72 DPI)
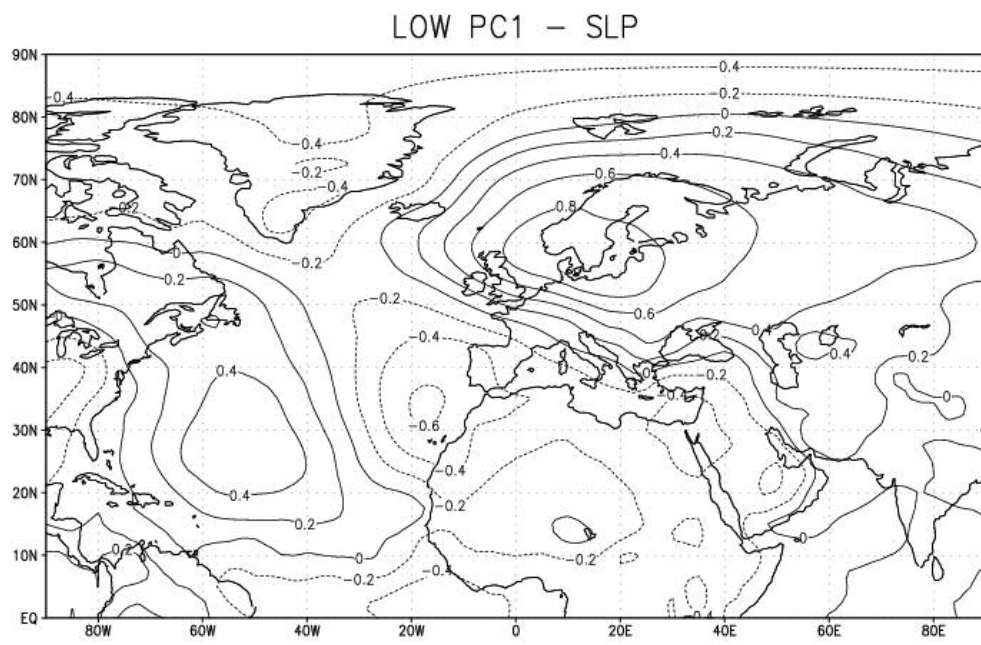
Figure 5. a)Composite map between PC1 (<-0.75) and SLP
246x160mm (72 x 72 DPI)
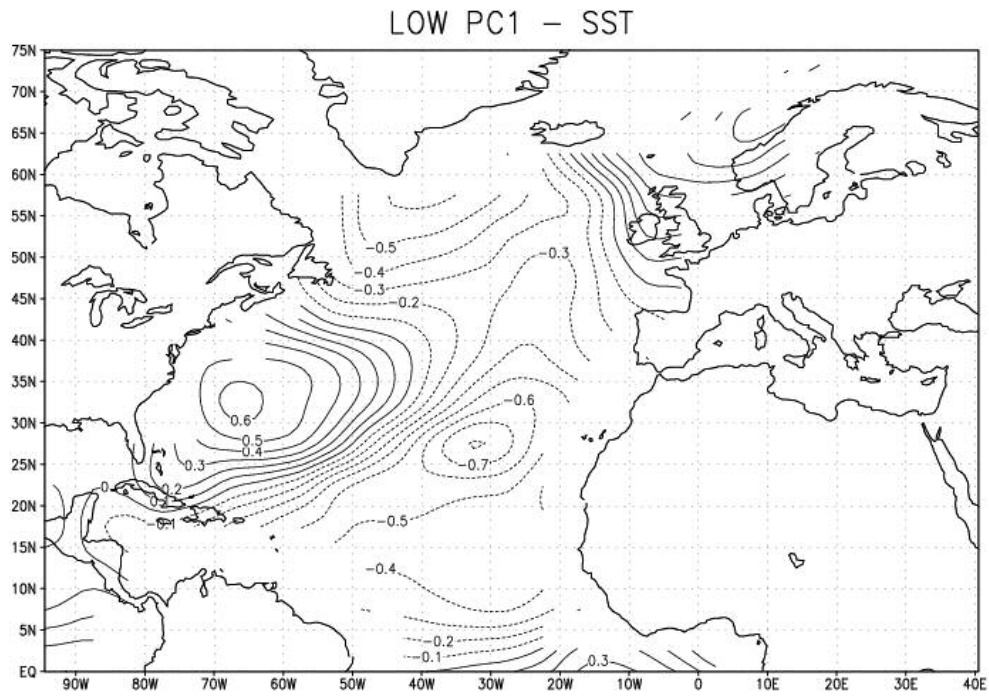
Figure 5. b) Composite map between PC1 (<-0.75) and SST
248x175mm (72 x 72 DPI)

Figure 6. a) Composite map between PC1 (>-0.75) and SLP
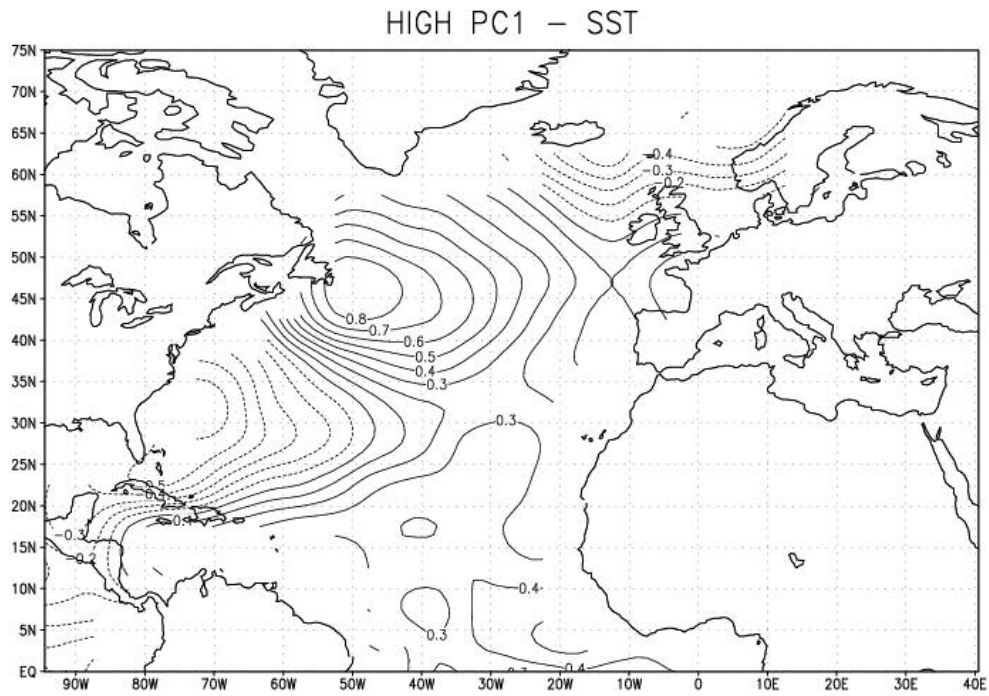246x160mm (72 x 72 DPI)

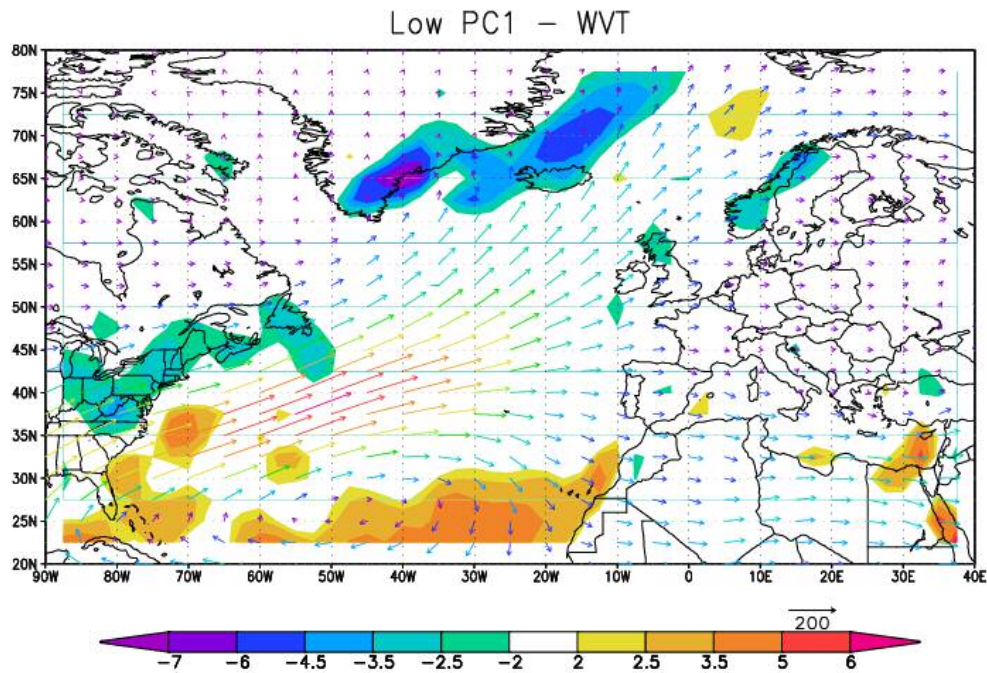**Figure 6. b) Composite map between PC1 (>-0.75) and SST**
248x175mm (72 x 72 DPI)

Figure 7. Composite maps of the vertically integrated water vapour transport for low (a) and high (b) values of PC1. Units are kg/(ms). The shaded areas indicate the distribution of the horizontal divergence of the total water vapour transport (units 10-6 kg/m2s)
249x171mm (72 x 72 DPI)

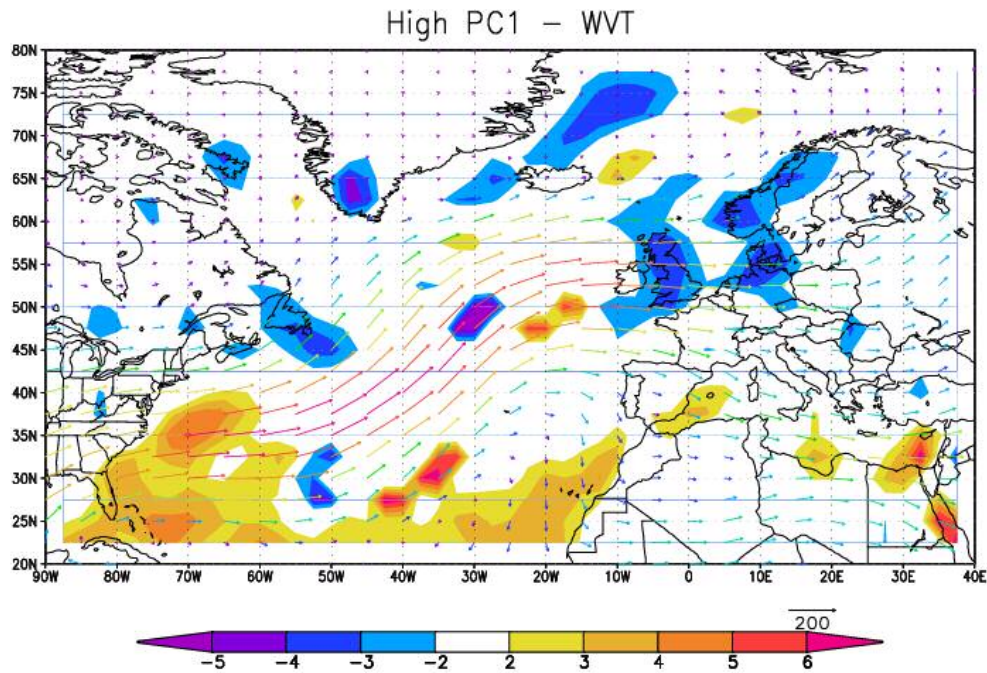**Figure 7. Composite maps of the vertically integrated water vapour transport for low (a) and high (b) values of PC1. Units are kg/(ms). The shaded areas indicate the distribution of the horizontal divergence of the total water vapour transport (units 10-6 kg/m2s)**
249x171mm (72 x 72 DPI)